Since January 2020 Elsevier has created a COVID-19 resource centre with free information in English and Mandarin on the novel coronavirus COVID-19. The COVID-19 resource centre is hosted on Elsevier Connect, the company's public news and information website.

Elsevier hereby grants permission to make all its COVID-19-related research that is available on the COVID-19 resource centre - including this research content - immediately available in PubMed Central and other publicly funded repositories, such as the WHO COVID database with rights for unrestricted research re-use and analyses in any form or by any means with acknowledgement of the original source. These permissions are granted for free by Elsevier for as long as the COVID-19 resource centre remains active.

ELSEVIER

Veterinary Immunology and Immunopathology
65 (1998) 243–257

Veterinary immunology and immunopathology

Cellular composition, coronavirus antigen expression and production of specific antibodies in lesions in feline infectious peritonitis

A. Kipar*, S. Bellmann, J. Kremendahl, K. Köhler, M. Reinacher

Institut für Veterinär-Pathologie, Universität Leipzig, Margarete Blank Strasse 4, 04103 Leipzig, Germany

Abstract

Twenty-three cats with spontaneous feline infectious peritonitis (FIP) were examined by light microscopy including immunohistology and histochemistry in order to determine the cellular composition and the expression of viral antigen in lesions in FIP. Furthermore, the presence of plasma-cells producing coronavirus-specific antibodies was evaluated in situ. Macrophages and neutrophils were demonstrated by an antibody against calprotectin (leukocyte protein L1, myeloid/histiocyte antigen), neutrophils were recognized due to their chloroacetate esterase activity, and B- and T-lymphocytes were identified by antibodies against the CD3 antigen and the CD45R antigen, respectively. Expression of viral antigen was immunohistologically demonstrated by a monoclonal antibody (mAb) against coronavirus while coronavirus-specific antibodies in situ were identified by the application of feline coronavirus prior to the coronavirus antibody. Lesions were classified as diffuse alterations at serosal surfaces, granulomas with areas of necrosis, granulomas without extended necrosis, focal and perivascular lymphoplasmocytic infiltrates, and granulomatous-necrotizing vasculitis. Diffuse alterations on serosal surfaces were represented either by activated mesothelial cells with single coronavirus antigen-bearing macrophages or by layers of precipitated exudate containing single to numerous granulomas with areas of necrosis. In liver and spleen, the exudate was often underlaid by a small band of subcapsular B-cells with an occasional plasma-cell producing coronavirus-specific antibodies. In other locations, a variably broad band of B-cells and plasma-cells, often infiltrating between underlying muscle fibers, separated the exudate from the unaltered tissue. Some of these plasma-cells were positive for coronavirus-specific antibodies. In granulomas with areas of necrosis, the central necrosis was surrounded by macrophages usually expressing considerable amounts of viral antigen. Few B-cells and plasma-cells were found in the periphery. In granulomas without extended necrosis, the number of macrophages were lower. Only few macrophages expressing low amounts of viral antigen were present. B-cells and plasma-cells formed a broad rim. Few plasma-cells stained positive for coronavirus-specific antibodies. In both types of granulomas, few neutrophils were found between macrophages. Few T-cells were seen scattered throughout the lesions. Focal and perivascular lymphoplasmocytic infiltrates were mainly

* Corresponding author. Tel. +49 341 9738278; fax: +49 341 9738299; e-mail: kipar@rz.uni-leipzig.de

0165-2427/98/$ – see front matter © 1998 Elsevier Science B.V. All rights reserved.
PII: S0165-2427(98)00158-5

seen in omentum and leptomeninx. B-cells were the predominant cells; some plasma-cells were positive for coronavirus-specific antibodies. Viral antigen was not readily detected in these alterations. Granulomatous-necrotizing vasculitis was occasionally found in kidneys and leptomeninx. It was dominated by macrophages which often stained strongly positive for coronavirus antigen. Different types of alteration were often seen in the same animal and even the same tissue. There was no obvious correlation between the cat's age, gross pathological changes, and the histological types of alteration. Single plasma-cells positive for coronavirus-specific antibodies were found around blood vessels distant from inflammatory alterations, within the lung parenchyma, as infiltrating cells in the mucosa of the small intestine, and in spleen and mesenteric lymph node. Results show that alterations in FIP are heterogeneous concerning cellular composition and expression of viral antigen. The dominance of B-cells in part of the lesions together with the presence of plasma-cells positive for coronavirus-specific antibodies indicate that these cells may play a role in the maintenance of inflammatory processes in FIP. © 1998 Elsevier Science B.V. All rights reserved.

Keywords: Feline infectious peritonitis; Immunohistology; Coronavirus antigen; Coronavirus-specific antibodies; B-cells; Plasma-cells

1. Introduction

The histopathological findings in spontaneous and experimental feline infectious peritonitis (FIP) have been described in several previous reports on effusive and non-effusive FIP (Wolfe and Griesemer, 1966; Montali and Strandberg, 1972; Ward et al., 1974; Hayashi et al., 1977, 1980). Although usually characteristic, both macroscopic and histological alterations were not always indicative of FIP. Therefore, differential diagnoses can sometimes not be readily excluded by routine post-mortem histopathology, and the diagnosis of FIP has to be confirmed by immunohistological demonstration of coronavirus antigen within the lesions (Tammer et al., 1995). We performed a systematic examination on the various lesions in naturally infected animals in order to further investigate cellular composition and content of immunohistologically detectable coronavirus antigen, and to detect the production of coronavirus-specific antibodies in situ.

2. Materials and methods

2.1. Animals and tissue processing

The study was performed on 23 cats with FIP. Animals had been routinely necropsied at the Department of Veterinary Pathology, Leipzig University, Leipzig, Germany. Tissue samples were fixed in 10% unbuffered, neutralized formalin for 16–18 h and were embedded in paraffin. Five μm-thick sections were either stained with hematoxylin–eosin or used for immunohistological and histochemical examinations.

Additionally, feline leukemia virus (FeLV) infection was diagnosed by immunohistology as described by Kovacevic et al. (1997).

2.2. Immunohistology

Immunohistology was performed on FIP lesions, lymphatic tissues (spleen and mesenteric lymph nodes), and bone marrow. Peroxidase-anti-peroxidase (PAP) and avidin–biotin peroxidase complex (ABC) methods were performed as described (Sternberger et al., 1971; Hsu et al., 1981).

Briefly, sections were deparaffinized in xylene and rehydrated through graded alcohols. Endogenous peroxidase was blocked by incubation with 0.3% hydrogen peroxide in methanol at room temperature for 30 min. Sections were washed with Tris-buffered saline (TBS, 0.1 M Tris–HCl with 0.9% NaCl, pH 7.6).

To demonstrate coronavirus antigen, sections were treated with target unmasking fluid (TUF; Dianova GmbH, Hamburg, Germany) for 10 min at 96°C. For the demonstration of the CD45R antigen of B-cells (Monteith et al., 1996), sections were incubated in citrate buffer (10 mM, pH 6.0) at 96°C for 30 min. To demonstrate the myeloid/histiocyte antigen of monocytes, macrophages, and neutrophils (leukocyte protein L1, calprotectin; Dale et al., 1983; Flavell et al., 1987) and the CD3 antigen of T-cells (Beebe et al., 1994), sections were pretreated with 0.5% protease (type XXIV: bacterial, Sigma Chemie Deisenhofen, Germany) diluted in phosphate-buffered saline (pH 7.2) at 37°C for 5 min.

After pretreatment, 50% swine serum in TBS were applied for 10 min at room temperature prior to rabbit anti-human CD3, while 10% rat serum in TBS were used prior to the monoclonal mouse antibodies and undiluted normal horse serum prior to rat anti-mouse CD45R, respectively.

Slides were then incubated for 12–16 h at 4°C with the primary antisera: mouse anti-coronavirus (FCV3-70; 1:100 in TBS; Custom Monoclonals International, West Sacramento, CA), mouse anti-human myeloid/histiocyte antigen (leukocyte protein L1, calprotectin; 1:1600 in TBS; Dako Diagnostika GmbH, Hamburg, Germany), rat anti-mouse CD45R (B220 (Ly5), clone RA3-6B2; 1:1000 in TBS; Cedar Lane Laboratories, Hornby, Canada), and rabbit anti-human CD3 (1:500 in 20% swine serum in TBS; Dako Diagnostika GmbH).

For rabbit anti-CD3, swine anti-rabbit IgG (1:100 in 20% swine serum in TBS; Dako Diagnostika GmbH) was used as a link antibody, followed by rabbit PAP complex (1:100 in 20% swine serum in TBS; Dako Diagnostika GmbH). For the mouse mAbs, rat anti-mouse IgG (1:100 in TBS; Dianova GmbH) and mouse PAP complex (1:500 in TBS; Dianova GmbH) were applied, while biotinylated rabbit anti-rat IgG (1:100 in TBS; Vector Laboratories, Burlingame, CA), followed by the ABC (A and B each 1:100 in TBS; Vector Laboratories) were used for the demonstration of the CD45R antigen. Incubations were performed at room temperature for 30 min each. Between each incubation step slides were washed with TBS.

Sections were incubated for 10 min with 0.05% 3,3′-diaminobenzidine tetrahydrochloride (DAB; Serva, Heidelberg, Germany) in 0.1 M imidazole/HCl buffer (pH 7.1) and counterstained with Papanicolaou's hematoxylin (1:20 in aqua dest.; E. Merck, Darmstadt, Germany).

For the demonstration of coronavirus-specific antibodies, slides were incubated with feline coronavirus (DF-2 FIPV; purified pelleted culture supernatant, 10-fold concentrated and stored in PBS; 1:25 in TBS) for 12–16 h at 4°C and washed with TBS prior to

the primary mouse anti-coronavirus antibody which was then detected by the PAP method as described above.

Negative controls for pAbs and mAbs were incubated with normal rabbit or rat serum or a non-reacting mouse mAb directed against chicken lymphocytes (Domingo et al., 1986), respectively. Negative controls for the detection of coronavirus-specific antibodies implied replacement of feline coronavirus by infectious bursitis disease virus (serotype I, purified, pelleted culture supernatant, 2-fold concentrated and stored in PBS; 1:25 in TBS), and either the application of the non-reacting mAbs directed against chicken lymphocytes mentioned above or a mouse anti-canine distemper virus mAb (DV2-12; 1:100 in TBS; Custom Monoclonals International) instead of the mouse anti-coronavirus mAb.

One case each of plasma cell-dominated gingivitis, conjunctivitis and otitis externa were examined for the presence of coronavirus antigen and plasma-cells producing coronavirus-specific antibodies.

Formalin-fixed and paraffin-embedded feline tissues (spleen, lymph nodes and bone marrow) served as positive controls for the leukocyte markers.

2.3. Histochemistry

In order to allow a clearcut differentiation of the cells in areas with caryorhexis, neutrophils were identified according to their chloroacetate esterase activity. The demonstration of the chloroacetate esterase was performed as previously described (Osbaldiston et al., 1978; Schaefer, 1983).

3. Results

3.1. Case histories and gross pathology

Animals ranged from 5 months to 6 years of age. Fourteen cats were male and nine were female. Reported clinical findings had been variable. In six cases, however, FIP was suspected. Information about the duration of the disease were available in three cases: animals had shown clinical symptoms for 2, 3, and 10 days, respectively.

Gross pathology was variable. Thirteen cats showed peritoneal effusion which was in one case accompanied by both pleural and pericardial effusion. Another three cats only exhibited pleural effusion and, in two of these cases, pericardial effusion. In most of the cases (n=18), fibrinous and/or granulomatous peritonitis was observed, involving abdominal wall, omentum, and the serosa of various tissues in a variable frequency. Eight of these cats showed parenchymal granulomas which were most often located in the kidney (n=7); another three cats exhibited necrotizing lymphadenitis of the mesenteric lymph nodes, and in further two cats fibrinogranulomatous pleuritis were additionally observed. Two animals showed pleuritis and pneumonia besides granulomatous hepatitis and lymphadenitis of the mesenteric lymph nodes or granulomatous hepatitis, nephritis, and leptomeningitis, respectively. In one cat each, lesions were restricted to fibrinous-granulomatous pleuritis and granulomas in both kidneys. Correlations between the cat's age and gross pathological findings could not be stated.

In 14 cats, FeLV co-infection was diagnosed by immunohistology.

3.2. Immunohistology and histochemistry of unaltered tissues

In lymphoid tissues, CD3 antigen-expressing T-lymphocytes, displaying a dark brown reaction at the cell periphery, were located in the paracortical region of lymph nodes and the periarteriolar sheath regions in the spleen. CD45R antigen-positive B-lymphocytes exhibited a similar staining pattern and were found in lymphoid follicles of lymph nodes and spleen. Monocytes, neutrophils, and macrophages showed a strong cytoplasmic staining for the myeloid/histiocyte antigen (leukocyte protein L1, calprotectin) in all tissues. Chloroacetate esterase activity was represented by a faint red cytoplasmic staining of neutrophils in tissues and myelomonocytic precursors in bone marrow, and a strong granular cytoplasmic staining of mast cells.

3.3. Light microscopy, immunohistology, and histochemistry in lesions of FIP

Staining for coronavirus antigen was represented by a granular precipitate in the cytoplasm of macrophages or, to a lesser extent, free within areas of necrosis (Figs. 1(a), 1(b) and Figs. 2, 3). After application of FIPV prior to the demonstration of coronavirus antigen, staining for both coronavirus antigen and coronavirus-specific antibodies were seen in the same slide (Figs. 1 and 4(a)). However, as the presence of coronavirus-specific antibodies were represented by an almost homogeneous cytoplasmic staining in plasma-cells which could be identified according to their morphology, both types of reaction were readily distinguishable (Figs. 1 and 4(a)).

Lesions were variable and were classified according to their distribution and cellular composition as diffuse alterations at serosal surfaces, granulomas with areas of necrosis,

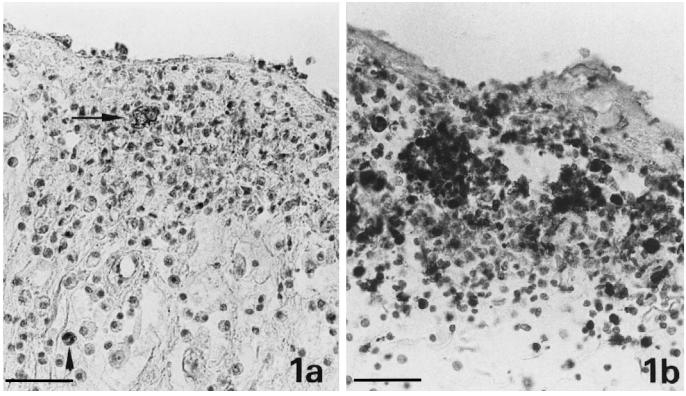

Fig. 1. Granuloma with area of necrosis in omentum. (a.) Coronavirus antigen in macrophages (granular reaction; arrow) within a granuloma with area of necrosis. Coronavirus-specific antibodies in plasma-cells close to the same granuloma (homogeneous reaction; arrowhead). Bar=40 μm. (b.) Macrophages expressing the myeloid/histiocyte antigen in a granuloma. Bar=40 μm.

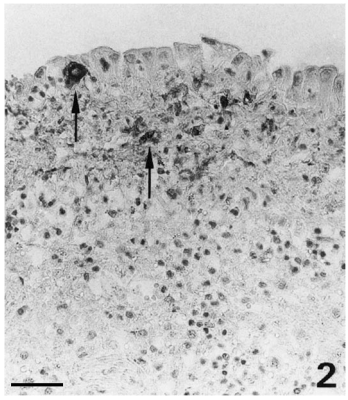

Fig. 2. Diffuse alteration at the serosal surface of the spleen. Activation of mesothelial cells and infiltration by macrophages expressing coronavirus antigen (arrows). Bar=40 μm.

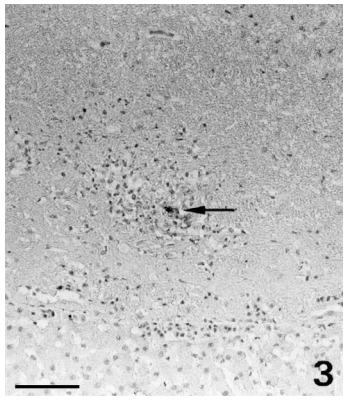

Fig. 3. Diffuse alteration at the serosal surface of the liver. Layers of exudate on serosal surface with focal infiltration by macrophages positive for coronavirus antigen (arrow). Bar=70 μm.

granulomas without extended necrosis, focal and perivascular lymphoplasmocytic infiltrates, and granulomatous-necrotizing vasculitis.

Diffuse alterations of serosal surfaces were variable. Mainly on the spleen, enlarged activated mesothelial cells, recognizable due to their cuboidal shape, were seen in combination with few macrophages in the edematous serosa (Fig. 2). Coronavirus antigen expression was restricted to the infiltrating macrophages (Fig. 2). On liver and spleen, layers of precipitated exudate containing few foci composed of macrophages which expressed variable amounts of viral antigen, were also seen (Fig. 3). Mainly in the liver, the protein exudate was underlaid by a small band of subcapsular B-cells and plasma-cells (Fig. 3). Occasionally, a single plasma-cell stained positive for coronavirus-specific antibodies. In many cases, serosal surfaces were covered with layers of precipitated exudate containing numerous granulomas with areas of necrosis. These granulomas were dominated by macrophages frequently only expressing small amounts

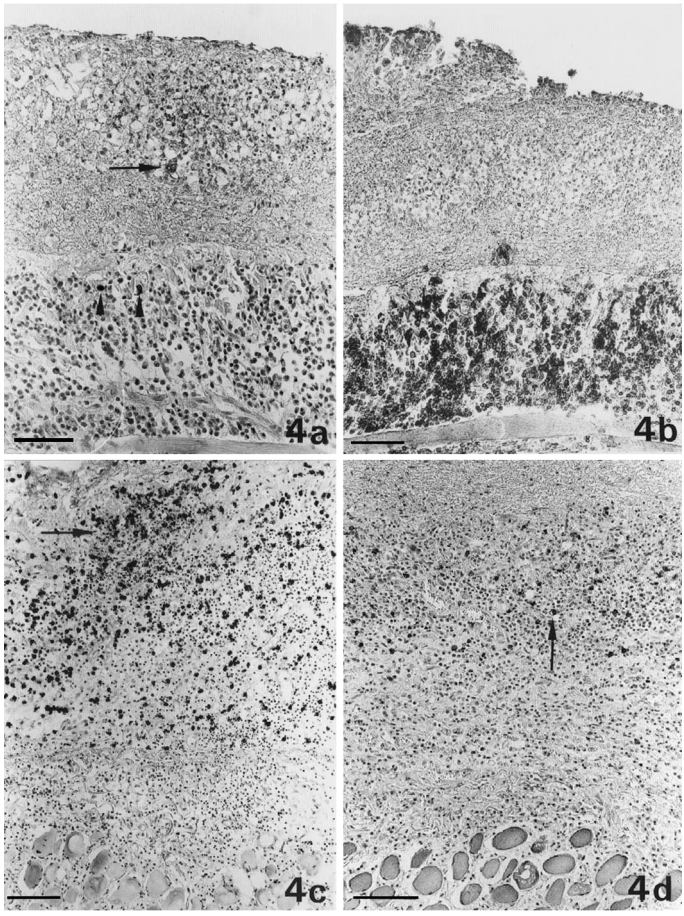

Fig. 4. Diffuse alteration at the serosal surface of the diaphragm. (a) Expression of coronavirus antigen in single macrophages (granular reaction; arrow) within a granuloma with area of necrosis; single plasma-cells positive for coronavirus-specific antibodies (homogeneous cytoplasmic reaction; arrowheads), are seen in the underlying layers of lymphocytes and plasma-cells. Bar=60 μm. (b) Layers of precipitated exudate with a granuloma are separated from the unaltered parenchyma by a thick layer of CD45R antigen-positive B cells and plasma-cells. Bar=40 μm. (c) Granuloma comprised mainly of macrophages, expressing the myeloid/histiocyte antigen (arrow) within the layers of exudate. Bar=100 μm. (d) CD3 antigen-positive T-cells (arrow) are rarely seen scattered throughout the lesion. Bar=100 μm.

of viral antigen (Fig. 4(a), (c)). Neutrophils were rarely seen. The precipitated exudate was separated from the unaltered parenchyma by few to many layers of B-cells and plasma-cells which occasionally infiltrated between underlying muscle fibers (Fig. 4(a), (b)); some of these plasma-cells were positive for coronavirus-specific antibodies (Fig. 4(a)). Few T-cells were scattered throughout the alteration (Fig. 4(d)). In some cases, diffuse almost pure B-cell and plasma-cell infiltration of pleura or peritoneum was seen. On the pleura, this was occasionally accompanied by proliferation of fibroblasts. These lesions contained single to numerous plasma-cells positive for coronavirus-specific

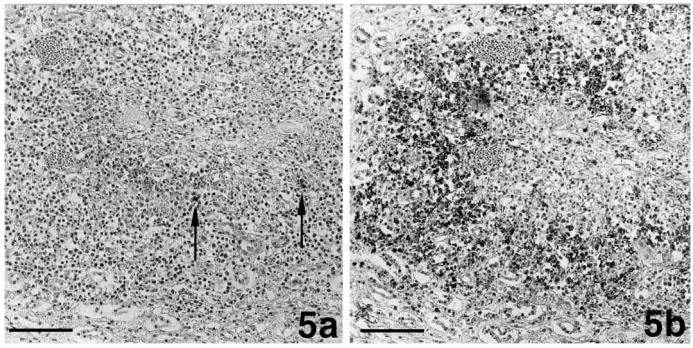

Fig. 5. Granuloma without extended necrosis in the renal medulla. (a.) Staining for coronavirus antigen in single macrophages within the center of focal granulomatous-necrotizing inflammation. Bar=80 μm. (b.) CD45R antigen-positive B-cells and plasma-cells are delineating the center of the same granuloma. Bar=90 μm.

antibodies. Viral antigen expression was in these cases restricted to single granulomas with areas of necrosis which were only detected after extended examination.

Granulomas with areas of necrosis were seen within diffuse alterations of the serosa (Fig. 4; see above), within the omentum, and within parenchymas (Fig. 1). A variably large area of central necrosis was surrounded by inflammatory cells which were almost completely identified as macrophages (Figs. 1(b) and 4(b)). Viral antigen expression were mostly restricted to a variable number of macrophages (Figs. 1 and 4(a)). Single to few neutrophils were scattered between macrophages. In the periphery of and close to the lesions, B-cells and plasma-cells were found; some of these plasma-cells stained positive for coronavirus-specific antibodies (Fig. 1(a)). Few T-cells were scattered throughout the granulomas.

Granulomas without extended areas of necrosis were mainly observed in the kidneys (Fig. 5). The small center comprised of macrophages which only rarely exhibited faint staining for viral antigen (Fig. 5(a)). They were intermingled with single neutrophils. The lesions were dominated by a broad rim of B-cells and plasma-cells (Fig. 5(b)); the latter were in part positive for coronavirus-specific antibodies. T-cells were again rare and scattered throughout the lesion.

Focal and perivascular lymphoplasmocytic infiltrates were mainly found in omentum and leptomeninx (Fig. 6); perivascular infiltrations were also seen occasionally in the brain of cats with granulomatous leptomeningitis (Fig. 7(a)). Some of the plasma-cells stained positive for coronavirus-specific antibodies (Figs. 6(b) and 7(a)). Macrophages and T- cells comprised a minority; neutrophils were rarely observed.

Granulomatous-necrotizing vasculitis was occasionally seen, mainly in the leptomeninx and the kidneys. Macrophages comprised the dominant cell population. They often showed a strong positive reaction for coronavirus antigen (Fig. 7(b)). Single to few neutrophils were seen in proximity to the vessel wall. T-cells were few and scattered throughout the infiltrates.

Different types of the lesions described above were frequently seen in the same animal and even in the same organ.

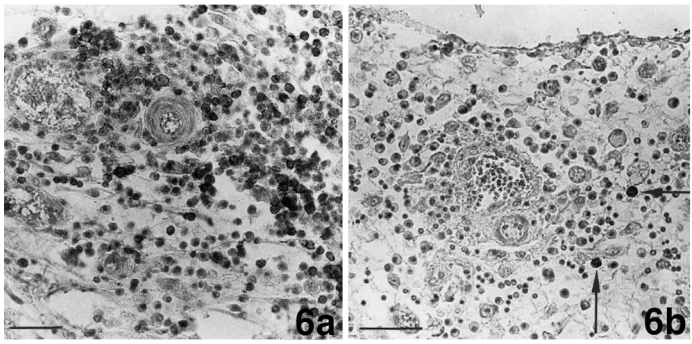

Fig. 6. Omentum. (a.) Infiltration of the omentum by CD45R antigen-positive B-cells and plasma-cells. Bar=40 μm. (b.) Single plasma cells positive for coronavirus-specific antibodies (arrows) are found in a perivascular infiltrate consisting of B- and plasma-cells. Bar=40 μm.

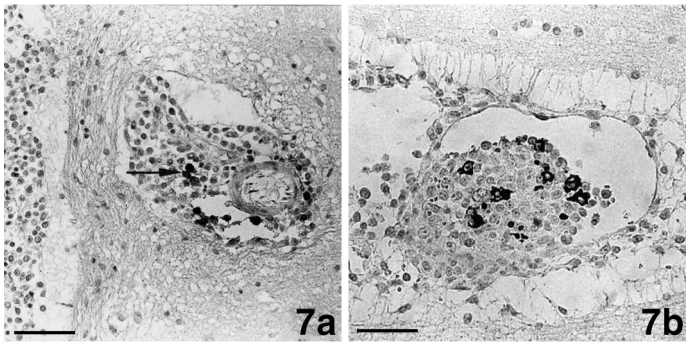

Fig. 7. Brain. (a.) Few plasma-cells positive for coronavirus-specific antibodies (arrow) are found in a mononuclear perivascular infiltrate in the neuropil close to the leptomeninx. Bar=80 μm. (b.) Granulomatous vasculitis. Part of the macrophages strongly express coronavirus antigen. Bar=40 μm.

Single plasma-cells producing coronavirus-specific antibodies were also found around blood vessels in tissues without further alterations: in the liver portal trias, the interstitium of the renal medulla, the lung, and the leptomeninx. They were also seen scattered in the wall of alveoli in the lungs and around bronchi. Furthermore, numerous plasma-cells producing coronavirus-specific antibodies were identified among infiltrating cells of the mucosa of the small intestine. Epithelial cells did not express coronavirus antigen.

Mesenteric lymph nodes without granulomatous-necrotizing lesions generally showed follicular hyperplasia with an increased number of CD45R antigen-positive B-cells and a large number of sinus histiocytes. They contained single to numerous plasma-cells positive for coronavirus-specific antibodies which were located in medullary cords and in or outside the lymph node capsule. In the paracortical T-cell zone the number of CD3 antigen-positive T-cells were slightly to moderately reduced. In the spleen, plasma-cells

with coronavirus-specific antibodies were rarely seen in the periphery of granulomatous-necrotizing lesions, within the subcapsular band of lymphocytes, and were diffusely disseminated. In spleens without granulomatous-necrotizing lesions, follicular hyperplasia and a slight reduction of T-cells in the periarteriolar sheath region was observed; viral antigen were not expressed.

Bone marrow was generally hyperplastic containing all cell lines. Part of the cells were positive for the CD3 or the CD45R antigen, respectively. In four cases, focal accumulations of B-cells were additionally seen. About half of the bone marrow cells expressed the myeloid/histiocyte antigen. In most cases, the number of neutrophils were mildly to massively increased. Neither coronavirus antigen nor plasma-cells positive for coronavirus-specific antibodies were found.

In three cases, information on the time period of clinical disease were available. The two cats showing clinical symptoms for 2 or 3 days prior to death exhibited fibrinous exudate on the peritoneum containing granulomas with areas of necrosis and moderate expression of viral antigen. Plasma-cells positive for coronavirus-specific antibodies were seen in the periphery of those lesions. The animal who had been ill for 10 days showed B-cell- and plasma-cell-dominated omentitis and serositis of the small intestine with few granulomas with areas of necrosis. Viral antigen were moderately expressed.

In many cases, mild to moderate B-cell-dominated focal interstitial infiltration of the renal cortex was found. There, neither viral antigen nor plasma-cells positive for coronavirus-specific antibodies were demonstrated.

Negative controls for leukocyte antigens and coronavirus antigen as well as for coronavirus-specific antibodies did not show any positive staining.

3.4. Immunohistology of control cases

In neither case of plasma cell-dominated inflammation (gingivitis, conjunctivitis and otitis externa) coronavirus antigen or plasma-cells positive for coronavirus-specific antibodies were found.

4. Discussion

Based on immunohistological and histochemical characterization of inflammatory cells as well as the presence of coronavirus antigen and plasma-cells producing coronavirus-specific antibodies in the lesions of 23 cats with spontaneous FIP, this study describes the composition of alterations observed in FIP after natural infection.

As previously described, coronavirus antigen can be demonstrated in FIP lesions by immunofluorescence or other immunohistological methods (Pedersen and Boyle, 1980; Tammer et al., 1995). We applied a coronavirus-specific mouse mAb usable on formalin-fixed and paraffin-embedded samples for immunohistology.

In this study, lesions which had first been generally described by Wolfe and Griesemer (1966), were classified according to their distribution and cellular composition. Diffuse alteration at serosal surfaces included activation of mesothelial cells and layers of precipitated exudate containing granulomas with areas of necrosis and macrophages

expressing viral antigen. B-cells and plasma-cells comprised underlying cell layers. There, some plasma-cells were positive for coronavirus-specific antibodies.

According to the amount of necrosis, granulomas were divided into those with areas of necrosis and those without extended necrosis. While the first were dominated by macrophages with only few surrounding B-cells and plasma-cells, the latter exhibited a small center with macrophages and a broad rim of B-cells and plasma-cells. Expression of viral antigen was nearly exclusively restricted to intact macrophages and were stronger in granulomas with areas of necrosis. In granulomas without extended necrosis, viral antigen was often not abundantly present, thereby rendering an immediate immunohistological diagnosis of FIP more difficult.

Single plasma-cells positive for coronavirus-specific antibodies were found in the periphery of and close to both types of granuloma.

Findings indicate that B-cells form a band between granulomas and unaltered tissue on serosal surfaces and progressively infiltrate granulomas, hence replacing macrophages. The presence of plasma-cells bearing coronavirus-specific antibodies between B-cells in close proximity to granulomas with necrosis and serosal exudate layers further indicates, that the immune response against the coronavirus starts before these FIP-specific alterations develop.

Focal accumulations and perivascular infiltrations of B-cells and plasma-cells were often observed in the omentum and sometimes in the leptomeninx. Some of these plasma-cells were positive for coronavirus-specific antibodies. This indicates that they represent a FIPV-specific immune response as it is also supported by the demonstration of plasma-cells bearing coronavirus-specific antibodies around blood vessels distant from granulomas. The presence of plasma-cells producing coronavirus-specific antibodies in cats with FIP in both lung tissue and intestinal mucosa without FIP lesions is presumably due to local immune response to oronasal coronavirus infection.

The immunohistological staining of macrophages in granulomas and acute vasculitis with a mAb against coronavirus indicates viral replication in macrophages. This has been demonstrated in cultivated macrophages (Jacobse-Geels and Horzinek, 1983) and by experimental studies which showed that aerosol application of FIPV results in infection of macrophages and persistent cell-associated viremia (Weiss and Scott, 1981a, b). Electron microscopical examinations demonstrated virus replication in peritoneal macrophages, mesothelial cells, and degenerating macrophages in inflammatory lesions (Zook et al., 1968; Hayashi et al., 1978; Weiss and Scott, 1981b). However, in our study, even activated mesothelial cells did not stain positive for coronavirus antigen.

Viral antigen was frequently not readily detectable in granulomas without extended necrosis where the number of macrophages were also comparatively low. The question then arises whether the remaining macrophages do not contain nearly any virus or whether the lower number of macrophages decreases only the statistical chance to detect viral antigen in immunohistology. It also seems possible that B-cells and plasma-cells totally replace macrophages, thereby leading to the development of mononuclear infiltrates as they are often seen in the renal cortex in cats with FIP regardless of their age. However, although these infiltrates were mainly comprised of B-cells, plasma-cells positive for coronavirus-specific antibodies were never seen in those infiltrates in this study.

T-cells comprised a minority in all types of lesions. The reason for this might be that T-cells do not play a major role in the pathogenesis of FIP lesions or that animals show a T-cell depletion. The latter was demonstrated in a previous study which also showed that T-cell depletion in FIP develops due to apoptosis (Haagmans et al., 1996).

Neutrophils were found among infiltrating cells in necrotizing lesions but were generally rarely seen. They did not contain viral antigen. This indicates that in FIP lesions neutrophils do not have a pathogenic role other than lysis of necrotic material.

Information on the time of alteration development in the experimentally induced FIP is not unequivocal and does not refer to the occurrence of lymphocytes and plasma-cells (Hayashi et al., 1980; Weiss and Scott, 1981b; Stoddart et al., 1988). In naturally infected animals, correlation between the duration of clinical disease and the various types of FIP lesions have not yet been evaluated (Wolfe and Griesemer, 1966).

In our study, the two cats showing 2 or 3 days of clinical disease prior to death exhibited fibrinous exudate containing granulomas with areas of necrosis on the peritoneum. Viral antigen was moderately expressed in granulomas, in the periphery of which few plasma-cells producing coronavirus-specific antibodies were seen. The animal which had been ill for 10 days showed B-cell- and plasma-cell-dominated omentitis and serositis at the small intestine with few granulomas with areas of necrosis. The increased presence of B- and plasma-cells could be interpreted as signs of a prolonged course of the disease. In general, obvious correlation between the cat's age, the presence of abdominal or pleural effusions, and the histological type of alterations could not be stated. On the contrary, the various types of lesions were frequently seen in the same animal and even in the same organ. It seems possible that natural FIP infection represents a slow disease progress with constant development of acute alterations, represented by granulomas with areas of necrosis. On the other hand, alterations might reflect different capacities of cellular immune response in affected cats.

The small band of subcapsular B-cells below layers of precipitated exudate was seen mainly in the liver. This might be the result of the cellular immune response which is focused on B-cells and macrophages.

All cats in our study showed follicular hyperplasia and sinus histiocytosis in lymphatic tissues as well as bone marrow hyperplasia as has been described previously (Wolfe and Griesemer, 1966; Montali and Strandberg, 1972; Hayashi et al., 1980).

In 14 cases, FeLV co-infection was diagnosed by immunohistology. FeLV infection is often accompanied by FIP (Cotter et al., 1975; Reinacher, 1989) and is, like other concurrent infections, considered as a potential predisposing factor for FCoV infection (Evermann et al., 1991). FeLV has been shown to permit the reactivation of FIP in healthy FCoV carriers (Pedersen, 1987). In our study, differences could not be stated between FeLV-positive and FeLV-negative cats with FIP concerning the expression of viral antigens, the number of plasma-cells producing coronavirus-specific antibodies, and the distribution and cellular composition of the lesions in FIP.

Summarizing the results of our study, one can state that FIP lesions are heterogenous as to their cellular composition and the intensity of viral antigen expression. Plasma-cells producing coronavirus-specific antibodies were present in the periphery and vicinity of granulomas. It does not seem unlikely, that granulomas develop from foci of centrally degenerating macrophages expressing coronavirus antigen. Neutrophils are rarely

intermingled. Few B-cells were seen in the periphery, but seem to progressively replace (degenerated) macrophages. The number of macrophages and the intensity of staining for coronavirus antigen decreases with the reduction of the areas of necrosis. Finally, B-cells obviously dominate focal lesions which are often devoid of coronavirus antigen.

FIP lesions are thought to be induced by immune complexes which are deposited at the wall of blood vessels, activate complement and damage vascular tissues. Furthermore, complement-mediated tissue damage may occur due to the binding of antibodies to viral antigen. Enhanced uptake into and thereby virus replication in macrophages may follow opsonization of FIPV by antibodies (Pedersen and Boyle, 1980; Weiss and Scott, 1981a, c; Weiss, 1994). This is corroborated by our finding that B-cells differentiating into plasma-cells which in part produce coronavirus-specific antibodies seem to play an important role in the maintenance of inflammatory processes in FIP.

The factors inducing B-cell accumulation and maturation of at least single B-cells into plasma-cells producing coronavirus-specific antibodies are not yet clearly defined. However, cultured peritoneal exudate cells (activated mesothelial cells, macrophages) from cats with FIP have been shown to release high amounts of IL-6 into the supernatant (Goitsuka et al., 1990). FIPV-infected alveolar macrophages and peritoneal exudate cells are known to produce IL-1 in situ (Goitsuka et al., 1987, 1988; Hasegawa and Hasegawa, 1991). IL-1 and IL-6 function as regulators of B-cell growth and differentiation and might therefore be responsible for maturation and immunoglobulin production of activated B-cells and plasma-cells in FIP lesions (Kishimoto, 1989; Goitsuka et al., 1987, 1988, 1990; Hasegawa and Hasegawa, 1991).

Acknowledgements

The authors wish to thank Mrs. R. Börner and Mrs. P. Herzog for technical assistance and Mr. R. Dobroschke for photographical assistance. We are grateful to Dr. Hermann Nieper, Institut für Virologie, Universität Leipzig, Leipzig, Germany, for kindly providing the feline coronavirus and infectious bursitis disease virus culture supernatants.

References

Beebe, A.M., Dua, N., Faith, T.G., Moore, P.F., Pedersen, N.C., Dandekar, S., 1994. Primary stage of feline immunodeficiency virus infection: viral dissemination and cellular targets. J. Virol. 68, 3080–3091.

Cotter, S.M., Hardy Jr., W.D., Essex, M., 1975. Association of feline leukemia virus with lymphosarcoma and other disorders in the cat. J. Am. Vet. Med. Assoc. 166, 449–454.

Dale, I., Fagerhol, M.K., Naesgard, I., 1983. Purification and partial characterization of highly immunogenic human leukocyte protein, the L1 antigen. Eur. J. Biochem. 134, 1–6.

Domingo, M., Reinacher, M., Burkhardt, E., Weiss, E., 1986. Monoclonal antibodies directed towards the two major cell populations in the Bursa of Fabricius of the chicken. Vet. Immunol. Immunopathol. 11, 305–317.

Evermann, J.F., McKeirnan, A.J., Ott, R.L., 1991. Perspectives on the epizootiology of feline enteric coronavirus and the pathogenesis of feline infectious peritonitis. Vet. Microbiol. 28, 243–255.

Flavell, D.J., Jones, D.B., Wright, D.H., 1987. Identification of tissue histiocytes on paraffin sections by a new monoclonal antibody. J. Histochem. Cytochem. 35, 1217–1226.

Goitsuka, R., Hirota, Y., Hasegawa, A., Tomoda, I., 1987. Release of interleukin-1 from peritoneal exudate cells of cats with feline infectious peritonitis. J. Vet. Med. Sci. 49, 811–818.

Goitsuka, R., Onda, C., Hirota, Y., Hasegawa, A., Tomoda, I., 1988. Feline interleukin-1 production induced by feline infectious peritonitis virus. Jpn. J. Vet. Sci. 50, 209–214.

Goitsuka, R., Ohashi, T., Ono, K., Yasukawa, K., Koishibara, Y., Fukui, H., Ohsugi, Y., Hasegawa, A., 1990. IL-6 activity in feline infectious peritonitis. J. Immunol. 144, 2599–2603.

Haagmans, B.T., Egberink, H.F., Horzinek, M.C., 1996. Apoptosis and T-cell depletion during feline infectious peritonitis. J. Virol. 70, 8977–8983.

Hasegawa, T., Hasegawa, A., 1991. Interleukin-1 alpha mRNA-expressing cells on the local inflammatory response in feline infectious peritonitis. J. Vet. Med. Sci. 53, 995–999.

Hayashi, T., Goto, N., Takahashi, R., Fujiwara, K., 1977. Systemic vascular lesions in feline infectious peritonitis. Jpn. J. Vet. Sci. 39, 365–377.

Hayashi, T., Goto, N., Takahashi, R., Fujiwara, K., 1978. Detection of coronavirus-like particles in a spontaneous case of feline infectious peritonitis. Jpn. J. Vet. Sci. 40, 207–212.

Hayashi, T., Utsumi, F., Takahashi, R., Fujiwara, K., 1980. Pathology of non-effusive type feline infectious peritonitis and experimental transmission. Jpn. J. Vet. Sci. 42, 197–210.

Hsu, S.M., Raine, L., Fanger, H., 1981. Use of avidin–biotin-peroxidase complex (ABC) in immunoperoxidase techniques. J. Histochem. Cytochem. 29, 577–580.

Jacobse-Geels, H.E.L., Horzinek, M.C., 1983. Expression of feline infectious peritonitis coronavirus antigens on the surface of macrophage-like cells. J. Gen. Virol. 64, 1859–1866.

Kishimoto, T., 1989. The biology of interleukin-6. Blood 74, 1–10.

Kovacevic, S., Kipar, A., Kremendahl, J., Teebken-Schuler, D., Grant, C.K., Reinacher, M., 1997. Immunohistochemical diagnosis of feline leukemia virus infection in formalin-fixed tissue. Eur. J. Vet. Pathol. 3, 13–19.

Montali, R.J., Strandberg, J.D., 1972. Extraperitoneal lesions in feline infectious peritonitis. Vet. Path. 9, 109–121.

Monteith, C.E., Chelack, B., Davis, W., Haines, D.M., 1996. Identification of monoclonal antibodies for immunohistochemical staining of feline B-lymphocytes in frozen and formalin-fixed paraffin-embedded tissues. Can. J. Vet. Res. 60, 193–198.

Osbaldiston, G.W., Sullivan, R.J., Fox, A., 1978. Cytochemical demonstration of esterases in peripheral blood leukocytes. Am. J. Vet. Res. 39, 683–685.

Pedersen, N.C., Boyle, J.F., 1980. Immunologic phenomena in the effusive form of feline infectious peritonitis. Am. J. Vet. Res. 41, 868–876.

Pedersen, N.C., 1987. Virologic and immunologic aspects of feline infectious peritonitis virus infection. Adv. Exp. Med. Biol. 218, 529–550.

Reinacher, M., 1989. Diseases associated with spontaneous feline leukemia virus (FeLV) infection in cats. Vet. Immunol. Immunopathol. 21, 85–89.

Schaefer, H.E., 1983. Histology and histochemistry in paraffin sections. Verh. Dtsch. Ges. Path. 67, 6–7.

Sternberger, L.A., Hardy Jr., P.H., Cuculis, C.C., Meyer, H.G., 1971. The unlabeled antibody-enzyme method for immunohistochemistry. Preparation and properties of soluble antigen–antibody-complex (Horseradish peroxidase–antihorseradish peroxidase) and its use in identification of spirochetes. J. Histochem. Cytochem. 18, 315–333.

Stoddart, M.E., Gaskell, R.M., Harbour, D.A., Pearson, G.R., 1988. The sites of early viral replication in feline infectious peritonitis. Vet. Microbiol. 18, 259–271.

Tammer, R., Evensen, O., Lutz, H., Reinacher, M., 1995. Immunohistological demonstration of feline infectious peritonitis virus antigen in paraffin-embedded tissues using feline ascites or murine monoclonal antibodies. Vet. Immunol. Immunopathol. 49, 177–182.

Ward, J.M., Gribble, D.H., Dungworth, D.L., 1974. Feline infectious peritonitis: Experimental evidence for its multiphasic nature. Am. J. Vet. Res. 35, 1271–1275.

Weiss, R.C., Scott, F.W., 1981a. Pathogenesis of feline infectious peritonitis: Nature and development of viremia. Am. J. Vet. Res. 42, 382–390.

Weiss, R.C., Scott, F.W., 1981b. Pathogenesis of feline infectious peritonitis: Pathologic changes and immunofluorescence. Am. J. Vet. Res. 42, 2036–2048.

Weiss, R.C., Scott, F.W., 1981c. Antibody-mediated enhancement of disease in feline infectious peritonitis: Comparisons with dengue hemorrhagic fever. Comp. Immun. Microbiol. Infect. Dis. 4, 175–189.

Weiss, R.C., 1994. Feline infectious peritonitis and other coronaviruses. In: Sherding, R.G. (Ed.), The cat: Diseases and Clinical Management, 2nd edn. vol. 1, Churchill Livingstone, New York, pp. 453–455.

Wolfe, L.G., Griesemer, R.A., 1966. Feline infectious peritonitis. Path. Vet. 3, 255–270.

Zook, B.C., King, N.W., Robison, R.L., McCombs, H.L., 1968. Ultrastructural evidence for the viral etiology of feline infectious peritonitis. Path. Vet. 5, 91–95.